

Article

Fabrication of Porous Al₂O₃ Ceramics with Submicron-Sized Pores Using a Water-Based Gelcasting Method

Zhihong Yang ¹, Nan Chen ^{1,*} and Xiaomei Qin ^{2,*}

¹ School of Materials Science and Engineering, Nanchang University, Nanchang 330031, China; yzhnc12@163.com

² Department of Physics, Shanghai Normal University, Shanghai 200234, China

* Correspondence: nanchen@ncu.edu.cn (N.C.); xmqin@shnu.edu.cn (X.Q.)

Received: 20 August 2018; Accepted: 18 September 2018; Published: 19 September 2018



Abstract: The gelcasting method is usually employed to fabricate relatively dense ceramics. In this work, however, porous Al₂O₃ ceramics with submicron-sized pores were fabricated using the water-based gelcasting method by keeping the Al₂O₃ content at low levels. By controlling the water content in the ceramic slurries and the sintering temperature of the green samples, the volume fractions and the size characteristics of the pores in the porous Al₂O₃ can be readily obtained. For the porous Al₂O₃ ceramics prepared with 30 vol.% Al₂O₃ content in the slurries, their open porosities were from 38.3% to 47.2%, while their median pore sizes varied from 299.8 nm to 371.9 nm. When there was more Al₂O₃ content in the slurries (40 vol.% Al₂O₃), the porous Al₂O₃ ceramics had open porosities from 37.0% to 46.5%, and median pore sizes from 355.4 nm to 363.1 nm. It was found that a higher sintering temperature and Al₂O₃ content in the slurries increased the mechanical strength of the porous Al₂O₃ ceramics.

Keywords: porous ceramics; Al₂O₃; submicron-sized pore; gelcasting

1. Introduction

Porous materials (including ceramic, metallic and polymeric types) are being developed and employed in different fields [1–14]. Among these types of porous materials, many researchers are investigating porous ceramics [1–9]. To date, many methods have been developed to prepare porous ceramics. Although the partial sintering of green bodies can result in porous ceramics, their properties are not usually desirable. In general, there are three types of processing techniques [15] that have been employed to fabricate porous ceramics: replica, sacrificial template, and direct foaming.

One of the most important methods for the replica technique is the freeze-casting method [16], in which ice crystals grow in a ceramic slurry to occupy spaces inside the ceramic body. During the freeze-drying process, these ice crystals are directly vaporized by vacuum sublimation and leave pores inside the ceramic green body. The freeze-casting technique is widely used to fabricate different types of porous ceramics [17–27]. However, the freeze-casting process, especially the freeze-drying stage, typically takes quite a long time and consumes much more electrical power. In addition, ice crystals usually grow into dendrites, which make the pore surfaces rough, and the porous ceramics often exhibit anisotropic properties.

Herein, a water-based gelcasting route is presented for fabricating porous Al₂O₃ ceramics with submicron pores, which could be used for filtration and other purposes. One of the advantages of the gelcasting method is that ceramics with complicated shapes can be readily fabricated [28,29]. In this method, high solid content in the ceramic slurries, or low water content, is usually needed to obtain

relatively dense ceramics [28,29]. The purpose of this work, however, is to prepare porous ceramics, rather than dense ceramics. Hence, in this work, the Al_2O_3 solid content is maintained at a relatively lower level, while the water content is kept at a relatively higher level in the ceramic slurries. Instead of freezing the water in the ceramic slurries into ice crystals, as in the freeze casting method [16], it is evaporated during the drying stage, and pores are retained in the green body. This allows porous Al_2O_3 ceramics with submicron pores to be successfully fabricated. It is noted that fabrication of porous ceramics with submicron pores using the gelcasting method has scarcely been reported in the literature.

2. Experimental

2.1. Material Preparation

Alpha Al_2O_3 powders (99.9% purity, grain size about 1 μm on average, Jiyuan Brother Materials Co. Ltd., Henan, China) were used in this study. The chemicals and fabrication method can be referred to in our previous work [30]. For the fabrication of porous ceramics in the present work, the Al_2O_3 content in the slurries was kept relatively low, at about 30–40 vol.%. In our previous work [30], however, the Al_2O_3 content in the slurries was about 55 vol.%, which is much higher than in the present work.

Figure 1 illustrates the processing steps for fabricating porous Al_2O_3 ceramics in this work. Ball-milled Al_2O_3 suspensions were poured into a metal mold (Figure 1a), and monomers were then polymerized to form crosslinked networks (Figure 1b) at 60 °C, for about 15 min. Then, the wet green bodies were dried at 70–110 °C and pores were retained (Figure 1c). The polymers within the dried green bodies were burnt out at 600 °C in air for 2 h. This process is called “degassing” (Figure 1d). These samples were then sintered in air at 1300 °C, 1350 °C and 1400 °C for 2 h to obtain porous Al_2O_3 ceramics (Figure 1e).

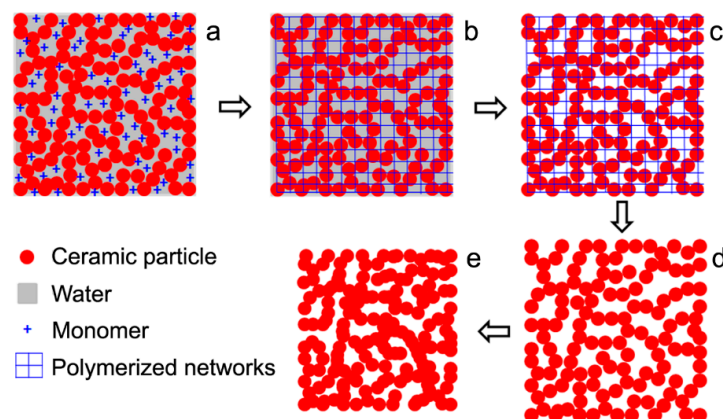


Figure 1. Fabrication steps of porous Al_2O_3 ceramics by gelcasting, (a) Al_2O_3 suspension; (b) polymerization of monomers; (c) drying; (d) burning out of polymers; and (e) sintering.

2.2. Material Characterization

The Archimedes method was used to measure the bulk densities of the porous Al_2O_3 ceramics, and their flexural strength was measured with an electronic universal testing machine (Sans Materials Testing Co. Ltd., Shanghai, China) under a three-point bending setup with a span length of 30 mm and a crosshead speed of 0.5 mm/min. The size of the sample was 3 mm \times 4 mm \times 36 mm. For the compressive strength test, the sample size was 5 mm in diameter and 10 mm in height, and it was measured with the same instrument and the same crosshead speed. The porosities and pore sizes of the Al_2O_3 porous ceramics were measured using the mercury porosimetry analysis method (AutoPore IV 9500, Micromeritics, Norcross, GA, USA).

A field emission scanning electron microscope (FESEM, Hitachi S4800, Tokyo, Japan) was used to investigate the microstructural characteristics of the porous Al_2O_3 ceramics. The Al_2O_3 particle size was analyzed using an image analysis software system (ImageJ, National Institutes of Health, Bethesda, MD, USA).

3. Results and Discussion

3.1. Microstructural Characteristics

Figures 2 and 3 show the microstructural morphologies of the porous Al_2O_3 ceramics, which were prepared with the Al_2O_3 content in the ceramic slurries with 30 vol.% (Figure 2) and 40 vol.% (Figure 3), respectively. The pore structures can be readily seen in Figures 2 and 3, and the Al_2O_3 particles can also be clearly identified. As shown in Figures 4 and 5, the Al_2O_3 particle size and the density of the porous Al_2O_3 ceramics steadily increased with the sintering temperature. This is generally expected for ceramics [31]. For the porous Al_2O_3 ceramics prepared with an Al_2O_3 content of 30 vol.% in the slurries, the particle size and density increased from about 1.03 μm and 1.96 g/cm^3 for sintering at 1300 $^\circ\text{C}$, to 1.52 μm and 2.24 g/cm^3 for sintering at 1400 $^\circ\text{C}$, respectively. For the porous Al_2O_3 ceramics prepared with Al_2O_3 content at 40 vol.% in the slurries, the particle size and the density increased from about 1.10 μm and 2.02 g/cm^3 for sintering at 1300 $^\circ\text{C}$, to 1.49 μm and 2.38 g/cm^3 for sintering at 1400 $^\circ\text{C}$, respectively.

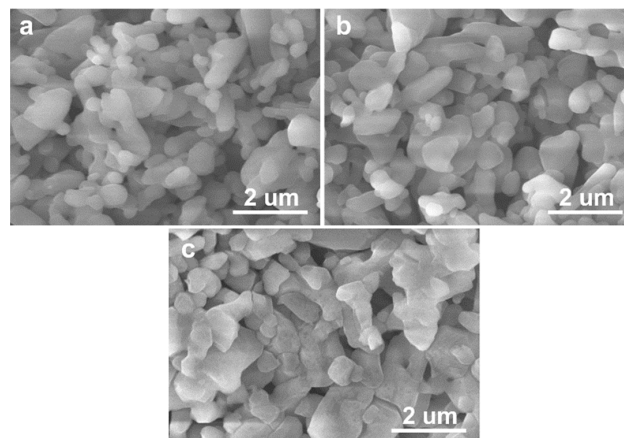


Figure 2. FESEM images of porous Al_2O_3 ceramics sintered at 1300 $^\circ\text{C}$ (a); 1350 $^\circ\text{C}$ (b) and 1400 $^\circ\text{C}$ (c), with the Al_2O_3 content at 30 vol.% in the ceramic slurries.

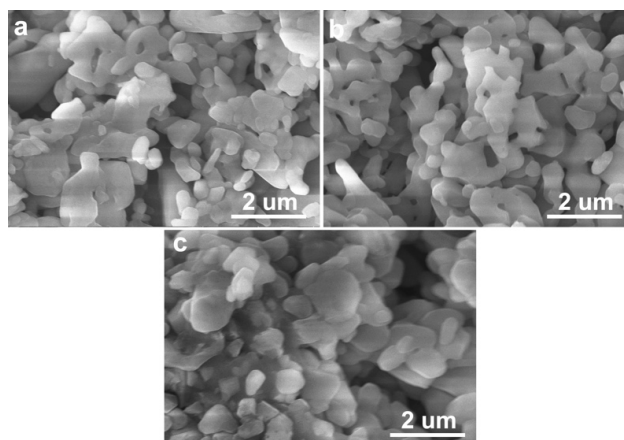


Figure 3. FESEM images of porous Al_2O_3 ceramics sintered at 1300 $^\circ\text{C}$ (a); 1350 $^\circ\text{C}$ (b) and 1400 $^\circ\text{C}$ (c), with the Al_2O_3 content at 40 vol.% in the ceramic slurries.

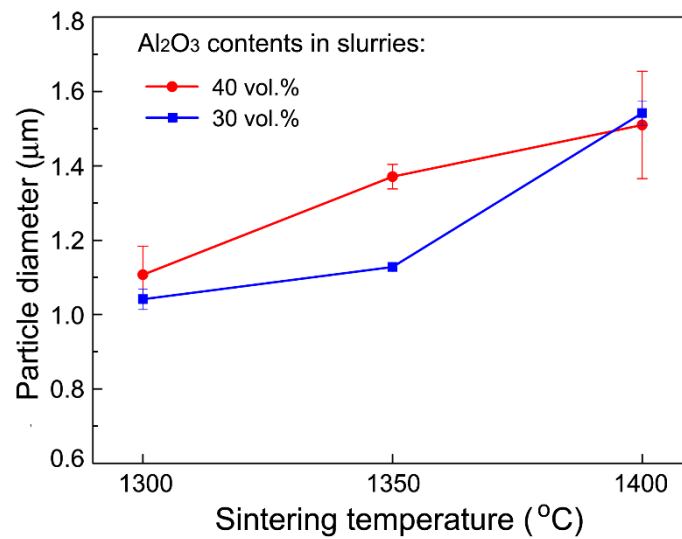


Figure 4. Variation of the particle diameter of porous Al₂O₃ ceramics with sintering temperature.

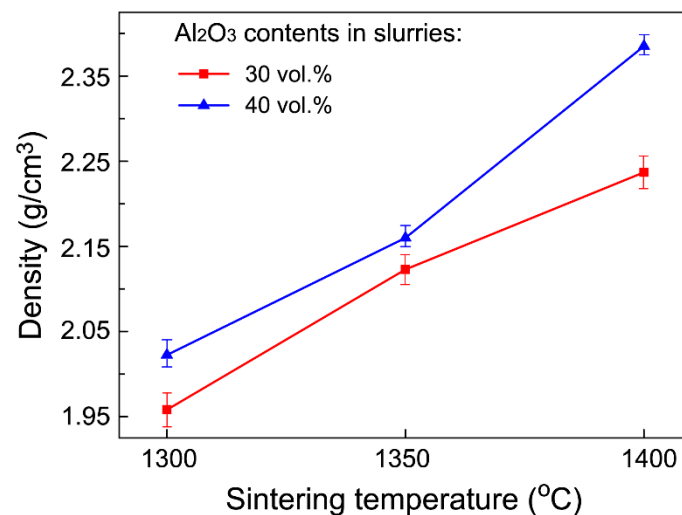


Figure 5. Variation of density of porous Al₂O₃ ceramics with sintering temperature.

Tables 1 and 2 list the porosities and median pore diameters of the porous Al₂O₃ ceramics prepared with the Al₂O₃ contents in the ceramic slurries at 30 vol.% (Table 1) and 40 vol.% (Table 2), respectively. Figure 6 shows the pore size distribution functions of the porous Al₂O₃ ceramics sintered at 1300 °C (Figure 6a) and 1400 °C (Figure 6b). It can be seen from Tables 1 and 2 that the porosity decreased with the sintering temperature. The closed porosities of the porous Al₂O₃ ceramics prepared with 40 vol.% Al₂O₃ content in the slurries were generally smaller than the samples prepared with 30 vol.% Al₂O₃ content in the slurries. In both of the two series of porous Al₂O₃ ceramics, the closed porosities were much smaller than the open porosities. This suggests that most of the pores in these samples were open pores [27]. This will be beneficial for filtration applications [1]. For the porous Al₂O₃ ceramics prepared with 30 vol.% Al₂O₃ content in the slurries, the median pore diameter decreased quickly from about 371.9 nm for sintering at 1300 °C, to about 299.8 nm for sintering at 1400 °C (Table 1). For the porous Al₂O₃ ceramics prepared with 40 vol.% Al₂O₃ content in the slurries, however, the pore diameter only slightly decreased (Table 2). The median pore diameter decreased from about 363.1 nm for sintering at 1300 °C, to about 355.4 nm for sintering at 1400 °C (Table 2). In fact, these results are in good agreement with the microstructural morphologies shown in Figures 2c and 3c. It can be noted that the pore size in Figure 3c of the 1400 °C-sintered porous Al₂O₃ ceramics prepared with 40 vol.%

Al_2O_3 content in the slurries was larger than that in Figure 2c of the 1400 °C-sintered porous Al_2O_3 ceramics prepared with 30 vol.% Al_2O_3 content in the slurries.

Table 1. Porosities and median pore diameters of porous Al_2O_3 ceramics (30 vol.% Al_2O_3 in the slurries).

Sintering Temperature (°C)	Open Porosity (%)	Closed Porosity (%)	Median Pore Diameter (nm)
1300	47.2	1.6	371.9
1350	42.5	2.2	330.6
1400	38.3	3.2	299.8

Table 2. Porosities and median pore diameters of porous Al_2O_3 ceramics (40 vol.% Al_2O_3 in the slurries).

Sintering Temperature (°C)	Open Porosity (%)	Closed Porosity (%)	Median Pore Diameter (nm)
1300	46.5	0.8	363.1
1350	41.7	1.9	358.5
1400	37.0	0.9	355.4

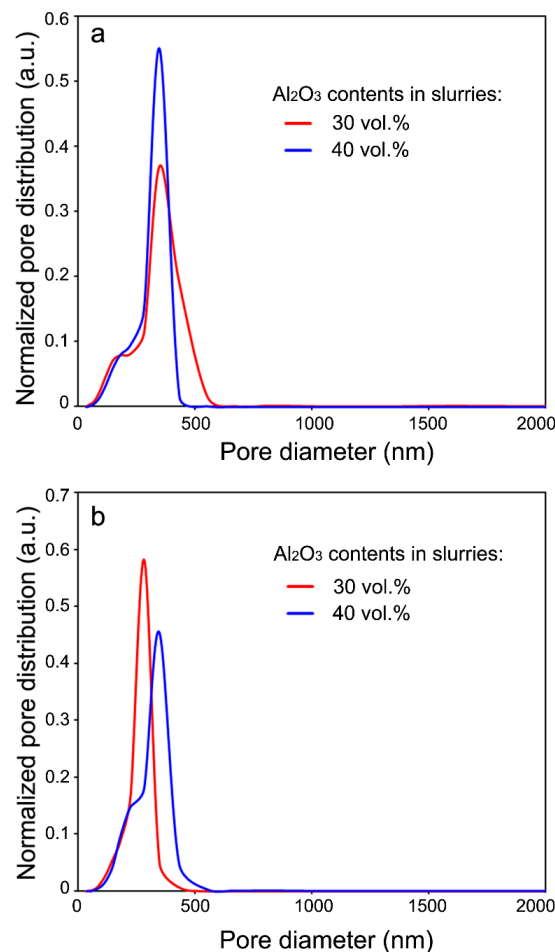


Figure 6. Normalized pore size distribution of porous Al_2O_3 ceramics for the sintering temperatures of 1300 °C (a) and 1400 °C (b).

3.2. Mechanical Properties

The flexural and compressive strength of the porous Al_2O_3 ceramics are shown in Figure 7. Figure 7a shows the dependence of the flexural strength of the porous Al_2O_3 ceramics on the sintering temperature. The flexural strength increased with the increasing sintering temperature. For the porous

Al_2O_3 ceramics prepared with Al_2O_3 content at 30 vol.% in the slurries, their flexural strength increased from 15.0 MPa when sintered at 1300 °C, to 36.2 MPa and 61.5 MPa when sintered at 1350 °C and 1400 °C, respectively. For the porous Al_2O_3 ceramics prepared with Al_2O_3 content at 40 vol.% in the slurries, their flexural strength increased from 19.6 MPa when sintered at 1300 °C, to 42.5 MPa and 73.1 MPa when sintered at 1350 °C and 1400 °C, respectively. Compared with our previous work on gelcasted Al_2O_3 ceramics [30], in which 55 vol.% Al_2O_3 content was used in the slurries, the porous Al_2O_3 ceramics of the present work had smaller flexural strength.

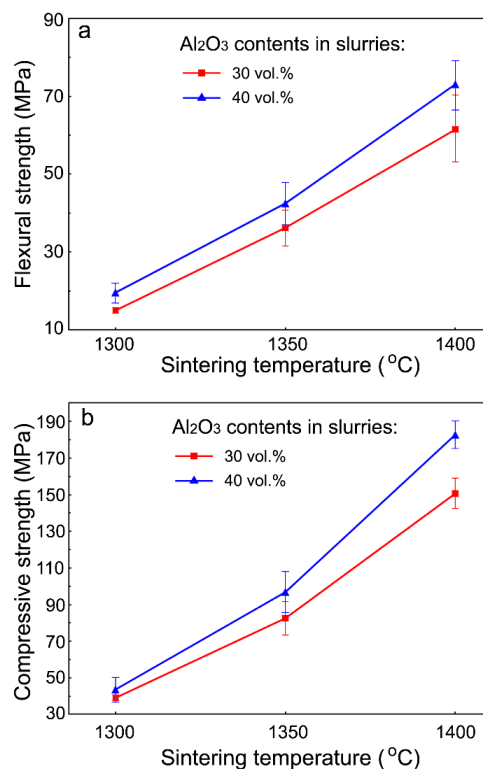


Figure 7. Variation of the flexural strength (a) and compressive strength (b) of porous Al_2O_3 ceramics with sintering temperature.

As shown in Figure 7a, in general, the porous Al_2O_3 ceramics prepared with 40 vol.% Al_2O_3 content in the slurries exhibited higher flexural strength than those prepared with 30 vol.% Al_2O_3 content in the slurries for all three sintering temperatures. Furthermore, the difference in their flexural strength became larger at the higher sintering temperature of 1400 °C (Figure 7a). This can be attributed to the larger total porosity of the porous Al_2O_3 ceramics prepared with 30 vol.% Al_2O_3 content in the slurries than those with 40 vol.% Al_2O_3 content in the slurries (Tables 1 and 2).

The compressive strength of the porous Al_2O_3 ceramics increased with the increasing sintering temperature (Figure 7b). This variation in behavior is similar to the flexural strength as shown in Figure 7a. For the porous Al_2O_3 ceramics prepared with Al_2O_3 content at 30 vol.% in the slurries, their compressive strength increased from 39.1 MPa when sintered at 1300 °C, to 82.6 MPa and 150.6 MPa when sintered at 1350 °C and 1400 °C, respectively. For the porous Al_2O_3 ceramics prepared with Al_2O_3 content at 40 vol.% in the slurries, their compressive strength increased from 43.6 MPa when sintered at 1300 °C, to 96.9 MPa and 182.8 MPa when sintered at 1350 °C and 1400 °C, respectively. Therefore, these porous Al_2O_3 ceramics are mechanically strong enough for practical applications. The dependence of their compressive strength on the sintering temperature (Figure 7b) is in agreement with the results of the Al_2O_3 /mullite composite porous ceramics reported by others [32]. However, the compressive strength of the porous Al_2O_3 ceramics of this work was consistently higher than the

Al₂O₃/mullite composite porous ceramics [32] and the porous Al₂O₃ ceramics prepared using carbon black as a pore former [33].

4. Conclusions

Porous Al₂O₃ ceramics with submicron pores were fabricated using the water-based gelcasting method. The open porosities and median pore sizes of the porous Al₂O₃ ceramics with 30 vol.% Al₂O₃ content in the slurries were 47.2% and 371.9 nm when sintered at 1300 °C, 42.5% and 330.6 nm when sintered at 1350 °C, and 38.3% and 299.8 nm when sintered at 1400 °C. The open porosities and median pore sizes of the porous Al₂O₃ ceramics with 40 vol.% Al₂O₃ content in the slurries were 46.5% and 363.1 nm when sintered at 1300 °C, 41.7% and 358.5 nm when sintered at 1350 °C, and 37.0% and 355.4 nm when sintered at 1400 °C. The porous Al₂O₃ ceramics exhibited high mechanical strength, which increased with both increasing sintering temperature and increasing Al₂O₃ content in the slurries.

Author Contributions: Conceptualization, N.C. and X.Q.; Methodology, X.Q.; Software, Z.Y.; Validation, Z.Y., N.C. and X.Q.; Formal Analysis, Z.Y., N.C. and X.Q.; Investigation, Z.Y.; Resources, N.C. and X.Q.; Data Curation, Z.Y.; Writing-Original Draft Preparation, Z.Y.; Writing-Review & Editing, N.C. and X.Q.; Visualization, Z.Y.; Supervision, N.C. and X.Q.; Project Administration, N.C.; Funding Acquisition, N.C. and X.Q.

Funding: This research was funded by the National Natural Science Foundation of China (grant numbers: 51362020, 11674231).

Acknowledgments: The authors are grateful to Wang and Hu for their assistance in the measurements of pore characteristics and mechanical properties of the samples.

Conflicts of Interest: The authors declare no conflicts of interest.

References

1. Hammel, E.C.; Ighodaro, O.L.-R.; Okoli, O.I. Processing and properties of advanced porous ceramics: An application based review. *Ceram. Int.* **2014**, *40*, 15351–15370.
2. Li, D.; Li, M. Porous Y₂SiO₅ Ceramic with low thermal conductivity. *J. Mater. Sci. Technol.* **2012**, *28*, 799–802. [[CrossRef](#)]
3. Sobsey, M.D.; Stauber, C.E.; Casanova, L.M.; Brown, J.M.; Elliott, M.A. Point of use household drinking water filtration: A practical, effective solution for providing sustained access to safe drinking water in the developing world. *Environ. Sci. Technol.* **2008**, *42*, 4261–4267. [[CrossRef](#)] [[PubMed](#)]
4. Heidenreich, S. Hot gas filtration—A review. *Fuel* **2013**, *104*, 83–94. [[CrossRef](#)]
5. Sundaram, S.; Colombo, P.; Katoh, Y. Selected emerging opportunities for ceramics in energy, environment, and transportation. *Int. J. Appl. Ceram. Technol.* **2013**, *10*, 731–739. [[CrossRef](#)]
6. Zhou, M.; Shu, D.; Li, K.; Zhang, W.Y.; Ni, H.J.; Sun, B.D.; Wang, J. Deep filtration of molten aluminum using ceramic foam filters and ceramic particles with active coatings. *Metall. Mater. Trans. A* **2003**, *34*, 1183–1191. [[CrossRef](#)]
7. Olson, R.A.; Martins, L.C.B. Cellular ceramics in metal filtration. *Adv. Eng. Mater.* **2005**, *7*, 187–192. [[CrossRef](#)]
8. Deville, S.; Saiz, E.; Tomsia, A.P. Freeze casting of hydroxyapatite scaffolds for bone tissue engineering. *Biomaterials* **2006**, *27*, 5480–5489. [[CrossRef](#)] [[PubMed](#)]
9. Moene, R.; Makkee, M.; Moulijn, J.A. High surface area silicon carbide as catalyst support characterization and stability. *Appl. Catal. A Gen.* **1998**, *167*, 321–330. [[CrossRef](#)]
10. Linul, E.; Movahedi, N.; Marsavina, L. On the lateral compressive behavior of empty and ex-situ Aluminum foam-filled tubes at high temperature. *Materials* **2018**, *11*, 554. [[CrossRef](#)] [[PubMed](#)]
11. Linul, E.; Movahedi, N.; Marsavina, L. The temperature and anisotropy effect on compressive behavior of cylindrical closed-cell aluminum-alloy foams. *J. Alloy. Compd.* **2018**, *740*, 1172–1179. [[CrossRef](#)]
12. Chang, S.; Li, L.; Lu, L.; Fuh, J.Y.H. Selective laser sintering of porous silica enabled by carbon additive. *Materials* **2017**, *10*, 1313. [[CrossRef](#)] [[PubMed](#)]
13. Tanaka, M.; Haniu, H.; Kamanaka, T.; Takizawa, T.; Sobajima, A.; Yoshida, K.; Aoki, K.; Okamoto, M.; Kato, H.; Saito, N. Physico-chemical, in vitro, and in vivo evaluation of a 3D unidirectional porous hydroxyapatite scaffold for bone regeneration. *Materials* **2017**, *10*, 33. [[CrossRef](#)] [[PubMed](#)]

14. Lee, H.-P.; Lin, D.-J.; Yeh, M.-L. Phenolic modified ceramic coating on biodegradable Mg alloy: The improved corrosion resistance and osteoblast-like cell activity. *Materials* **2017**, *10*, 696. [[CrossRef](#)] [[PubMed](#)]
15. Studart, A.R.; Gonzenbach, U.T.; Tervoort, E.; Gauckler, L.J. Processing routes to macroporous ceramics: A review. *J. Am. Ceram. Soc.* **2006**, *89*, 1771–1789. [[CrossRef](#)]
16. Liu, R.; Xu, T.; Wang, C.-A. A review of fabrication strategies and applications of porous ceramics prepared by freeze-casting method. *Ceram. Int.* **2016**, *42*, 2907–2925. [[CrossRef](#)]
17. Sofie, S.W.; Dogan, F. Freeze casting of aqueous alumina slurries with glycerol. *J. Am. Ceram. Soc.* **2001**, *84*, 1459–1464. [[CrossRef](#)]
18. Fukasawa, T.; Deng, Z.-Y.; Ando, M.; Ohji, T.; Goto, Y. Pore structure of porous ceramics synthesized from water-based slurry by freeze-dry process. *J. Mater. Sci.* **2001**, *36*, 2523–2527. [[CrossRef](#)]
19. Araki, K.; Halloran, J.W. Porous ceramic bodies with interconnected pore channels by a novel freeze casting technique. *J. Am. Ceram. Soc.* **2005**, *88*, 1108–1114. [[CrossRef](#)]
20. Koh, Y.H.; Sun, J.J.; Kim, H.E. Freeze casting of porous Ni–YSZ cermets. *Mater. Lett.* **2007**, *61*, 1283–1287. [[CrossRef](#)]
21. Chen, R.; Wang, C.-A.; Huang, Y.; Ma, L.; Lin, W. Ceramics with special porous structures fabricated by freeze-gelcasting: Using tert-butyl alcohol as a template. *J. Am. Ceram. Soc.* **2007**, *90*, 3478–3484. [[CrossRef](#)]
22. Deville, S.; Saiz, E.; Nalla, R.K.; Tomsia, A.P. Freezing as a path to build complex composites. *Science* **2006**, *311*, 515–518. [[CrossRef](#)] [[PubMed](#)]
23. Zhang, H.; Fidelis, C.L.; Serva, A.L.T.; Wilhelm, M.; Rezwani, K. Water-based freeze casting: Adjusting hydrophobic polymethylsiloxane for obtaining hierarchically ordered porous SiOC. *J. Am. Ceram. Soc.* **2017**, *100*, 1907–1918. [[CrossRef](#)]
24. Fukushima, M.; Yoshizawa, Y.-I. Fabrication and morphology control of highly porous mullite thermal insulators prepared by gelation freezing route. *J. Eur. Ceram. Soc.* **2016**, *36*, 2947–2953. [[CrossRef](#)]
25. Tang, Y.; Qiu, S.; Wu, C.; Miao, Q.; Zhao, K. Freeze cast fabrication of porous ceramics using tert-butyl alcohol–water crystals as template. *J. Eur. Ceram. Soc.* **2016**, *36*, 1513–1518. [[CrossRef](#)]
26. Xu, T.; Wang, C.-A. Effect of two-step sintering on micro-honeycomb BaTiO₃ ceramics prepared by freeze-casting process. *J. Eur. Ceram. Soc.* **2016**, *36*, 2647–2652. [[CrossRef](#)]
27. Liu, X.; Xue, W.; Shi, C.; Sun, J. Fully interconnected porous Al₂O₃ scaffolds prepared by a fast cooling freeze casting method. *Ceram. Int.* **2015**, *41*, 11922–11926. [[CrossRef](#)]
28. Franks, G.V.; Tallon, C.; Studart, A.R.; Sesso, M.L.; Leo, S. Colloidal processing: Enabling complex shaped ceramics with unique multiscale structures. *J. Am. Ceram. Soc.* **2017**, *100*, 458–490. [[CrossRef](#)]
29. Leo, S.; Tallon, C.; Stone, N.; Franks, G.V. Near-net-shaping methods for ceramic elements of (body) armor systems. *J. Am. Ceram. Soc.* **2014**, *97*, 3013–3033. [[CrossRef](#)]
30. Hu, Y.; Du, G.; Chen, N. A novel approach for Al₂O₃/epoxy composites with high strength and thermal conductivity. *Compos. Sci. Technol.* **2016**, *124*, 36–43.
31. Barsoum, M.W. *Fundamentals of Ceramics*; McGraw Hill: New York, NY, USA, 1997.
32. Sun, Z.; Fan, J.; Hu, P.; Ding, F.; Yang, J.; Yuan, F. A novel low-temperature strategy for synthesis of alumina ceramics with uniform and interconnected pores by silica coating. *J. Mater. Sci.* **2017**, *52*, 1603–1616. [[CrossRef](#)]
33. Liu, J.; Li, Y.; Li, Y.; Sang, S.; Li, S. Effects of pore structure on thermal conductivity and strength of alumina porous ceramics using carbon black as pore-forming agent. *Ceram. Int.* **2016**, *42*, 8221–8228. [[CrossRef](#)]

